Published in final edited form as:

Cancer Res. 2017 June 15; 77(12): 3169–3180. doi:10.1158/0008-5472.CAN-16-2787.

Plk1 Phosphorylation of Mre11 Antagonizes the DNA Damage Response

Zhiguo Li[1], **Jie Li**[1], **Yifan Kong**[2], **Shan Yan**[3], **Nihal Ahmad**[4], and **Xiaoqi Liu**[1,5,*]

[1]Department of Biochemistry, Purdue University, West Lafayette, IN 47907

[2]Department of Animal Sciences, Purdue University, West Lafayette, IN 47907

[3]Department of Biological Sciences, University of North Carolina, Charlotte, NC 28223

[4]Department of Dermatology, University of Wisconsin, Madison, WI 53706

[5]Center for Cancer Research, Purdue University, West Lafayette, IN 47907

Abstract

The mitotic kinase Plk1 contributes to the DNA damage response (DDR) by targeting multiple factors downstream of the core responder kinase ATM/ATR. In this study, we show that Plk1 also phosphorylates key factors upstream of ATM/ATR and regulates their DDR-related functions. Plk1 phosphorylated Mre11, a component of the Mre11/Rad50/Nbs1 (MRN) complex, at serine 649 (S649) during DDR. Phosphorylation of Mre11-S649 by Plk1 primed subsequent CK2-mediated phosphorylation at Mre11-serine 688 (S688). Phosphorylation of Mre11 at S649/S688 inhibited loading of the MRN complex to damaged DNA, leading to both premature DNA damage checkpoint termination and inhibition of DNA repair. Tumors expressing phosphomimetic Mre11 were more sensitive to the PARP inhibitor olaparib, compared to those expressing unphosphorylatable Mre11, suggesting that patients with elevated Plk1 expression might benefit from olaparib treatment.

Keywords

Plk1; Mre11; phosphorylation; DNA damage response

Introduction

Although it has been well documented that Polo-like kinase 1 (Plk1) has critical roles in many mitotic events (1,2), mounting evidence suggests that Plk1 is also involved in many non-mitotic events, including DNA damage response (DDR) (3) and G2 DNA damage checkpoint recovery (4). Throughout the life of an organism, the integrity of genome is continuously challenged by DNA lesions due to exposure to both exogenous (genotoxic chemicals or radiation) or endogenous (normal metabolic byproducts or DNA replication) agents. The DDR pathway is essential for the maintenance of genomic stability. The DDR

*To whom correspondence should be addressed: Dr. Xiaoqi Liu, Department of Biochemistry, Purdue University, 175 S. University Street, West Lafayette, IN 47907 Tel: 765-496-3764; Fax: 765-494-7897; liu8@purdue.edu.

cascade can be broadly divided into two phases: an early cascade comprising recruitment of the Mre11-Rad50-Nbs1 (MRN) complex, autoactivation of ATM/ATR, and generation of γ-H2AX, followed by a later cascade, induced by RNF8 that mediates the retention of RNF168, BRCA1 and 53BP1 (5). Upon activation, ATM/ATR phosphorylate a large number of substrates to regulate various downstream pathways. Cells have evolved multiple pathways in response to DNA damage that span from arrest of the cell cycle progression (DNA damage checkpoint), repair of the DNA lesions (DNA repair), to the re-establishment of cellular homeostasis (checkpoint recovery). The DNA lesions are first sensed by the multifunctional MRN complex, which in turn activates ATM/ATR and triggers DNA damage response. There are two major competing pathways for repair of DNA double-strand breaks (DSBs): homologous recombination (HR) and non-homologous end-joining (NHEJ). Mre11 has both endo- and exonuclease activities against a variety of single-stranded DNA (ssDNA) and double-stranded DNA (dsDNA) substrates (6,7) and these nuclease activities contribute to both HR (8) and NHEJ (9). Of note, it was reported that Plk1 also directly phosphorylates the Rad51 recombinase and facilitates HR in response to DSBs (10).

In order to have enough time to repair DNA lesions, cells will activate the checkpoint pathway to stop cell cycle. Activated ATM and ATR phosphorylate checkpoint effector kinases Chk2/1, which subsequently phosphorylate substrates including Cdc25, resulting in inactivation of Cdk1. ATM and ATR also directly phosphorylate Bora which is recognized and degraded by E3 ligase $SCF^{\beta TRCP}$ (11). Once Bora is destructed, mitotic entry is restricted by Cdk1/Cyclin B inhibition partially due to Plk1 inactivation (12). DNA damage-induced cell cycle arrest will allow cells to repair damaged DNA. Upon completion of DNA repair, the checkpoint has to be silenced to restart cell cycle progression. Compared to activation of the DNA damage checkpoint and repair, the exact mechanism of checkpoint recovery is poorly understood. Previous work showed that Plk1 plays a crucial role during recovery from G2 DNA damage checkpoint (4). Further, the activity of Plk1 is required for inactivation of the ATR/Chk1 pathway through phosphorylation-induced degradation of ATR-mediator protein Claspin (13). Recently, it has been shown that Plk1 inactivates the ATM-Chk2 pathway through phosphorylation of 53BP1 and Chk2 (14). In response to G2 DNA damage, p53 pathway is also activated to lead to cell-cycle arrest. Plk1-associated activity inactivates p53 by phosphorylating GTSE1, a negative regulator of p53 (15). Collectively, the studies summarized above revealed an essential role of Plk1 in checkpoint recovery by targeting multiple factors downstream of ATM and ATR. Whether Plk1 regulates functions of proteins upstream of ATM and ATR is not known.

Overexpression of Plk1, observed in many cancers, has often been correlated with disease stage, histologic grade, poor prognosis, metastatic potential and survival (1). Consequently, several Plk1 inhibitors have been developed, with some agents showing encouraging results in various cancer cell lines and xenograft models of human cancer (16,17). Of these, volasertib (BI6727) has been most extensively studied clinically. In contrast to marked antitumor activity in multiple cancer models, overall antitumor activity of volasertib in patients with solid tumor has been modest in trials (16). To fully understand the role of Plk1 in the context of IR-induced carcinogenesis, we need dissect how Plk1-associated kinase activity regulates DDR and its subsequent repair in more details.

Materials and Methods

Cell culture, transfections, and RNAi

HeLa, U2OS, HCT116 and HEK293T cells were cultured in DMEM supplemented with 10% fetal bovine serum (FBS), 100 units/ml penicillin, and 100 units/mL streptomycin at 37˚C in 8% CO_2. Cell lines were obtained from ATCC in 2006. Additional cell line authentication and mycoplasma testing have not been tested after its purchase. The numbers of passages of cells used in the study were below 20. Plasmid transfections were performed with Liopfectamine (Invitrogen), whereas siRNA was transfected with Transmessenger transfection reagent (QIAGEN). Cells were examined at 30 hours after transfection for immunoblotting. The pKD-CK2 construct used to deplete CK2 was obtained from Upstate. The following target sequence was used to design siRNA against human Plk1: AAGGGCGGCTTTGCCAAGTGCTT. To deplete Mre11, oligonucleotides with the following sense and antisense sequences were used for the cloning of small-hairpin RNA (shRNA)-encoding sequences in lentiviral vector: 5′-GATCCCCGGCACTGAGAAACAT GCAATTCAAGAGAT TGCATGTTTCTCAGTGCCTTTTTGGAAA-3′ (sense) and 5′-AGCTTTTCCAAAAAGGCAC T GAGAAACATGCAATCTCTTGAATTGCATGTTTCTCAGTGCCGGG-3′ (antisense).

Antibodies

The phospho-specific antibodies against Mre11-S649 and Mre11-S688 were generated by Proteintech. In brief, two peptides containing phospho-S649 and phospho-S688 were synthesized and used to immunize rabbits. After the antibodies were affinity purified, a series of control experiments were performed to confirm its specificity. The antibodies against ATM (NB100-104) and phospho-ATM (p-S1981) (NB100-81803) are from Novus Biologicals. The antibodies against Nbs1 (GTX70224), and Rad50 (GTX70228) were purchased from GeneTex. The antibodies against phospho-Chk2 (p-T68) (2661), Chk2 (2662), Mre11 (4847), and CK2 (2656) were obtained from Cell Signaling. The antibodies against γ-H2AX (ab22551) were from Abcam, whereas the antibodies against Plk1 (05-844) were from Millipore.

Synchronization and checkpoint assay

Cells were incubated with thymidine (2.5 mmol/L) for 16 hours to arrest at the G1/S transition. Thymidine was washed away throughly to release cells into fresh medium. At 8 hours post-release, the second round of thymidine were added to arrest cells at the G1/S boundary. Where indicated, the G2/M DNA damage checkpoint was activated by treating cells with 0.5 μmol/L doxorubicin for 1 hour at 7 hours post-release from the double thymidine block (DTB). In order to inactivate DNA damage signaling and allow mitotic entry, caffeine (5 mmol/L) was added to inhibit ATM and ATR checkpoint kinases.

Recombinant protein purification

Various GST-tagged human Mre11 constructs were subcloned into pGEX-KG, expressed in E. coli, and purified. Point mutations were generated using the QuickChange Site-Directed Mutagenesis Kit (Stratagene). To purify Plk1 kinase, Hi5 insect cells were infected with

baculovirus encoding GST-Plk1 and harvested 36 hr after infection. Recombinant GST-fusion proteins were affinity-purified by incubation with glutathione-agarose beads, followed by extensive washes with STE buffer (10 mmol/L Tris-HCl, pH 8.0, 1 mmol/L EDTA, 150 mmol/L NaCl) and elution with glutathione elution buffer (40 mmol/L glutathione, 50 mmol/L Tris-HCl, 10 mmol/L DTT, 200 mmol/L NaCl, pH 8.0).

In vitro kinase assay

In vitro kinase assays were performed in TBMD buffer (50 mmol/L Tris [pH 7.5], 10 mmol/L $MgCl_2$, 5 mmol/L dithiothreitol, 2 mmol/L EGTA, 0.5 mmol/L sodium vanadate, 20 mmol/L p-nitrophenyl phosphate) supplemented with 125 μmol/L ATP and 10 μCi of [γ-32P] ATP at 30°C for 30 minutes in the presence of GST-Mre11 proteins. After the reaction mixtures were resolved by SDS-PAGE, the gels were stained with Coomassie brilliant blue, dried, and subjected to autoradiography.

Xenopus egg extracts

The use and care of Xenopus laevis were approved by the Institutional Animal Care and Use Committee (IACUC) of the University of North Carolina at Charlotte. Low-speed supernatant egg extract was prepared according to our previously published approach (18).

Electrophoretic mobility shift assay (EMSA)

Double-stranded DNA (dsDNA) end binding of proteins was assessed by EMSA as described previously (19). Oligonucleotides were chemically synthesized and purified by HPLC (IDT). The sequences of oligonucleotides were: TP423: 5′- CTG CAG GGT TTT TGT TCC AGT CTG TAG CAC TGT GTA AGA CAG GCC AGA TC-3′; and TP424: 5′- CAC AGT GCT ACA GAC TGG AAC AAA AAC CCT GCA GTA CTC TAC TCA TCT C- 3′. After the 5′ end of TP423 was labelled with [γ-^{32}P]ATP and polynucleotide kinase (New England Biolabs), TP423 and TP424 oligonucleotides were annealed to generate the 3′ overhanging DNA duplexes. After the 3′ overhanging DNA duplexes (10 pmol/L) were subsequently incubated with purified Mre11 (10 nmol/L) proteins in the binding buffer [25 mmol/L MOPS, pH 7.0, 60 nmol/L KCl, 0.2% Tween, 2 mmol/L DTT, 1 mmol/L $Mg(CH_3COO)_2$] at 73˚C for 15 minutes, gel loading buffer [250 mmol/L Tris-HCl (pH 7.5), 0.2% bromphenol blue and 40% glycerol] was added to the reaction. The reaction products were separated on a 5% non-denaturing polyacrylamide gel at 4 °C in Tris borate/EDTA buffer for 2 hours. After the gels were dried and exposed to the phosphorimaging screen, images were acquired using Typoon FLA 9500 and subsequently by autoradiography.

Comet assay

After irradiation, the 0.5% agarose microgel with embedded cells was placed into the lysis buffer containing 2.5 M NaCl, 0.1 M EDTA, 10 mmol/L Tris base, and 1% Triton X-100 (pH 12.5), at 4°C for 1 hour. Thereafter, slides were equilibrated with fresh electrophoresis buffer (0.3 mol/L NaOH, 1 mmol/L EDTA) for 40 minutes in order to unwind DNA, and then electrophoresed for 30 minutes at 25 V. The nucleoids were subsequently washed in neutralizing buffer (0.4 mol/L Tris-HCl, pH 7.5), before staining with DAPI (5 μg/mL) (20).

Animal experiments

All procedures involving mice were guided by Purdue University Animal Care and Use Committee (Protocol no: 1111000133E001). Mice, housed in the animal facility with free access to standard rodent chow and water, were under pathogen-free conditions and maintained in a 12 hours light/12 hours dark cycle. To generate tumors, U2OS cells (3×10^6 cells per mouse) were mixed with an equal volume of Matrigel (Collaborative Biomedical Products) and inoculated into the right flank of nude mice (Harlan Laboratories). Two weeks later, animals were randomized into treatment and control groups with six mice each. Olaparib (50 mg/kg) was injected into the tail vein twice weekly. Tumor volumes were measured by formula: $V = L \times W^2/2$ [V is volume mm^3;), L is length (mm), W is width (mm)]. Tumors were fixed in 10% neutral buffered formalin, paraffin embedded, sectioned to 5 μmol/L, and stained using conventional hematoxylin and eosin (H&E) staining.

Statistical Analysis

All data are presented as means ± standard deviation (SD). Statistical calculations were performed with Microsoft Excel analysis tools. While a two-tailed, unpaired student's t test was used to assess the difference between the effects of treatment in cell lines, one-way analysis of variance was used to determine statistically significant differences from the means in the animal study. P values of <0.05 were considered statistically significant. *p<0.05, **p<0.01.

Results

Plk1 suppresses DDR by inactivation of the ATM/Chk2 pathway

To dissect how Plk1-associated kinase activity affects DDR, we first assessed the status of H2AX phosphorylation at S139 (γ-H2AX) following IR treatment in cells treated with BI2536, a Plk1 inhibitor (21). As shown in Fig. 1A and Fig. S1A, BI2536 pre-treatment significantly increased IR-induced γ-H2AX formation in U2OS cells. Next, U2OS cells were transfected with different forms of Plk1 (constitutively active T210D or kinase dead K82M mutant) and subjected to IR. Cells expressing Plk1-KM showed much high levels of γ-H2AX staining than cells expressing Plk1-TD mutant (Fig. 1B). Phosphorylation of Sgt1, a previously identified Plk1 substrate (22), was used as a control to indicate the kinase activity of Plk1. Furthermore, to understand how Plk1 regulates γ-H2AX formation due to IR, we sought to determine whether Plk1 is involved in the events upstream of H2AX phosphorylation. It has been established that the formation and expansion of γ-H2AX at DSB sites depends on activation of ATM kinase (23). Therefore, we asked whether there is a functional link between Plk1 and ATM during DDR by modulation of Plk1 activity. Pre-treatment of cells with BI2536 significantly increased IR-induced phosphorylation, thus activation of ATM and its downstream target Chk2 (Fig. 1C and S1B–D). Similarly, Plk1 knockdown by siRNA also markedly increased IR-induced phosphorylation and activation of ATM and Chk2 (Fig. 1D and S1E). To further confirm the critical role of Plk1 in IR-induced activation of the ATM/Chk2 pathway, we also compared DDR in cells expressing different forms of Plk1. Upon IR, cells expressing Plk1-T210D showed reduced levels of phospho-ATM and phospho-Chk2 than cells expressing Plk1-K82M (Fig. 1E, S1F and G).

Collectively, these data support the notion that Plk1-associated kinase activity antagonizes IR-induced activation of ATM and its downstream targets Chk2 and H2AX.

Plk1 phosphorylates Mre11 at S649

To dissect how Plk1 is involved in DDR, we first used the *Xenopus* egg extract system, in which DDR signaling can be reconstituted in vitro (24). Extracts prepared from *Xenopus* egg were treated with different forms of Plk1 proteins. Consistent with the findings in intact cells, pre-treatment with constitutive active Plk1 markedly inhibited ATM autophosphorylation induced by dsDNA without altering ATM levels (Fig. 2A). Because the MRN complex is recruited to DNA DSBs before ATM activation by autophosphorylation, we tested the hypothesis that Plk1 prevents ATM activation via its direct phosphorylation towards the MRN complex. Accordingly, DNA-bound proteins were isolated from the egg extract, followed by in vitro kinase assay with purified Plk1 ± BI2536. As indicated in Fig. 2B, a protein with the size of 85 kDa, the molecular weight of Mre11, was phosphorylated by Plk1, suggesting that Mre11 might be a direct target of Plk1. In a separate search for novel Plk1-interacting proteins using mass spectrometry, we also identified Mre11 as a potential Plk1 substrate (25). To directly test whether Mre11 is a substrate of Plk1, a series of in vitro kinase assays were performed with purified Plk1 and various recombinant glutathione S-transferase (GST)-fused Mre11 regions in the presence of [γ-^{32}P]ATP. As indicated, Plk1 directly phosphorylates the very C-terminal region of Mre11-aa 623–709 (Fig. 2C). Further, site-directed mutagenesis was used to identify S649 and S688 as two major phosphorylation sites in vitro (Fig. 2D). To confirm the kinase/substrate relationship, two phospho-specific antibodies (pS649 and pS688) were generated. A series of control experiments were performed to characterize the specificity of the two antibodies. Purified GST-Mre1-aa 623-709 (WT, S649A, S688A) was incubated with Plk1 in the presence of unlabeled ATP, followed by anti-pS649 and anti-pS688 IB. As indicated, S649A and S688A mutations completely abolished the respective anti-pS649 and anti-pS688 Western signals, indicating that the antibodies recognize only phosphorylated forms of Mre11 at those two sites (Fig. 2E). Next, HEK293T cells expressing GFP-Mre11 (WT, S649A, S688A) were analyzed by IB with the two antibodies. Both pS649 and pS688 signals were detected in cells expressing Mre11-WT, but not in cells expressing Mre11-S649A or -S688A, respectively (Fig. 2F), indicating that both sites are phosphorylated in vivo. To test whether Plk1 is the kinase responsible for the two phosphorylation sites in vivo, Plk1 inhibitor BI2536 was used to inhibit Plk1 kinase activity. The pS649, but not the pS688, epitope of endogenous Mre11 in 293T cells was substantially reduced when cells had been pre-treated with BI2536 (Fig. 2G). Conversely, phosphorylation of S649 and S688 of Mre11 significantly increased as cells enter mitosis in a well-synchronized culture, matching the expression level of Plk1 (Fig. 2H). Next, we asked whether other mitotic kinases are also responsible for these phosphorylation events. Accordingly, cells were arrested at mitosis by nocodazole and harvested after incubation with different protein kinase inhibitors (Fig. S2A). Treatment with three Plk1 inhibitors BI2536, BI6727 or GSK461364 all impaired the phosphorylation of Mre11-S649. In contrast, the phosphorylation level of Mre11-S649 was not affected by treatment with Aurora A inhibitor I or RO-3306, a Cdk1/2 inhibitor, suggesting that endogenous Mre11 is phosphorylated at S649 in a Plk1-dependent manner.

CK2 is responsible for Mre11-S688 phosphorylation in vivo

Although Plk1 phosphorylates Mre11-S688 in vitro (Fig. 2D), inhibition of Plk1 did not significantly affect Mre11-S688 phosphorylation in vivo (Fig. 2G). It has been established that both Plk1 and CK2 prefer a target sequence containing negatively charged residues nearby and that two kinases share the same sites in some substrates (26,27). Therefore, we examined the ability of CK2 to phosphorylate Mre11-S688. In vitro kinase assays revealed efficient phosphorylation of GST-Mre11-WT, but not GST-Mre11-S688A, by CK2 (Fig. 2I). Notably, inhibition of CK2 activity with its inhibitor TBCA greatly reduced the pS688 epitope in 293T cells (Fig. 2J), indicating that CK2 is the major kinase responsible for Mre11-S688 phosphorylation. To further confirm these results, RNAi-mediated Plk1 or CK2 depletion was performed. As indicated, depletion of Plk1 abolished the pS649 epitope, but not the pS688 epitope. In contrast, the pS688, but not the pS649 epitope, was substantially reduced when CK2 was depleted (Fig. 2K). Thus, we concluded that Plk1 phosphorylates Mre11-S649 and that CK2 targets Mre11-S688 in vivo.

Phosphorylation of Mre11 by Plk1 and CK2 is required for G2 DNA damage checkpoint recovery

Next, to examine whether the effect of Plk1-associated kinase activity on IR-induced activation of ATM and its downstream targets Chk2 and H2AX is dependent on Mre11-S649 phosphorylation, we reconstituted Mre11-depleted cells with Mre11-S649A mutant. We found that complementation with Mre11-S649A mutant in Mre11-depleted cells blocked BI2536-induced IR sensitivity (Fig. S2B and C). Because Mre11 phosphorylation at S649/S688 is clearly cell cycle regulated (Fig. 2H), we asked whether Mre11 is involved in normal mitotic progression by Mre11 knockdown using siRNA targeting the 3′ UTR. As a control, we found that Plk1-depleted cells accumulated with a 4 N DNA content, indicating a G2/M arrest of these cells. In contrast, no difference in FACS profile or Cyclin B level was observed upon Mre11 depletion (Fig. S3A), indicating that loss of Mre11 does not interfere with normal mitotic progression. Because Plk1 plays a central role in G2 DNA damage checkpoint recovery and because Mre11 is an initial DNA damage response protein, we next tested whether Mre11-S649/S688 phosphorylation affects G2 DNA damage checkpoint recovery. Toward this end, we synchronized U2OS cells at the G1/S boundary using the DTB and then allowed cells to progress through the cell cycle. At 7 hours after release, a time at which the majority of cells had completed S phase (Fig. S3B), cells were treated with IR to induce DNA damage during G2 phase (Fig. 3A). Strikingly, we found that treatment of cells with IR had reduced Mre11 phosphorylation at S649 and S688 without affecting the level of Mre11 (Fig. 3B). Of note, phosphorylation of Plk1-T210 and Sgt1 was inhibited by IR, indicating that Plk1 is inactivated upon DNA damage (Fig. 3B). Subsequently, we mimicked checkpoint silencing by addition of ATM/ATR checkpoint kinase inhibitor caffeine to override the DNA damage checkpoint thus to follow checkpoint recovery. As shown in Fig. 3C, DNA damage induced by doxorubicin blocked the cells into mitosis and treatment with caffeine drove the cells to reenter mitosis. By contrast, Plk1 inhibition with BI2536 prevented caffeine-induced mitotic re-entry, suggesting that Plk1 activity is required for G2 DNA damage checkpoint recovery (Fig. 3C and S3C). Similarly, we found that levels of pS649 and pS688 were considerably reduced in the presence of doxorubicin compared with untreated samples (Fig. 3D). In contrast, enhanced phosphorylation at S649/S688 was

detected during the caffeine-induced checkpoint recovery, but remained to be either unphosphorylated at S649 or weakly phosphorylated at S688 in the presence of BI2536 (Fig. 3D), suggesting that the phosphorylation of S649/S688 during the G2 checkpoint recovery is Plk1 dependent. This result is consistent with the outcome described above in unperturbed cell, where the level of pS688 was slightly reduced upon Plk1 depletion (Fig. 2K), indicating that Plk1 is also involved in phosphorylation of Mre11 at S688. We also noticed that the pS688 epitope was apparently reduced in Mre11-S649A mutant background in vitro (Fig. 2E) and in vivo (Fig. 2F), and that the intensity of the pS688 epitope in cells expressing Mre11-S649D obviously increased (Fig. S3D). Of note, several studies previously indicated that Plk1 and CK2 can act in concert to regulate one substrate (10,26). Therefore, we evaluated whether Plk1 phosphorylation at S649 might modify the efficiency of CK2-mediated phosphorylation at S688 by using of sequential kinase assays. We first incubated GST-Mre11-aa 623-709 immobilized on glutathione beads with Plk1 or CK2, after washing off the kinase, a second kinase reaction was carried out. Strikingly, pre-phosphorylation of Mre11 with Plk1 substantially facilitated subsequent phosphorylation by CK2, indicated by a significantly increased level of the pS688 epitope. In contrast, CK2-prephosphorylation of Mre11 did not alter the efficiency of Plk1-dependent phosphorylation of Mre11 at S688 (Fig. 3E). These results support the notion that during DNA damage checkpoint recovery Mre11 is sequentially modified by Plk1-dependent priming phosphorylation at S649, followed by CK2-mediated phosphorylation at S688.

If the observed mitotic phosphorylation of Mre11 is critical for the G2 DNA damage checkpoint recovery, we would expect to observe altered kinetics of G2/M transition when the phosphorylation site mutants of Mre11 are expressed under genotoxic condition. To directly examine whether Mre11-S649/S688 phosphorylation is involved in checkpoint recovery, endogenous Mre11 was replaced with RNAi-resistant Mre11 constructs (WT, S649A or S688A), and subjected to DNA damage and recovery process as above. Cells expressing Mre11-WT were able to recovery from G2 arrest (Fig. 3F, left). In contrast, cells expressing Mre11-S649A or -S688A showed recovery defects (Fig. 3F, middle and right). Further, the levels of pS649 and pS688 were considerably reduced in the presence of doxorubicin compared to untreated samples. In contrast, significantly enhanced phosphorylation at S649/S688 was detected during the caffeine-induced checkpoint recovery (Fig. 3F, left). Interestingly, Mre11-S649A mutation apparently blocked caffeine-induced phosphorylation of S688 (Fig. 3F, middle), further confirming that the priming phosphorylation of S649 by Plk1 is required for the subsequent phosphorylation of S688 by CK2 during the checkpoint recovery. Although Mre11-S688A mutation did not affect caffeine-induced phosphorylation of S649 by Plk1, cells expressing Mre11-S688A failed to enter mitosis, arguing that CK2-mediated phosphorylation at S688 is also critical for checkpoint recovery (Fig. 3F, right). Consistent with this observation, inhibition of CK2 activity partially prevented caffeine-induced mitotic re-entry after DNA damage (Fig. S3E). Because the polo-box domain (PBD) has been responsible for interacting with most of known Plk1 substrates, we also performed co-IP analysis for GFP-Mre11 with different domains of Flag-Plk1. As indicated, the PBD but not the kinase domain of Plk1 interacts with Mre11 (Fig. S3F).

Mre11 phosphorylation at S649/S688 inhibits its binding to dsDNA and antagonizes the ATM signaling

Mre11 has two potential DNA-binding-domain (DBDs) with S649/S688 located within the second DBD (Fig. S4A) (28). Therefore, we speculated that Mre11-S649/S688 phosphorylation might modulate its ability to load onto DNA. To explore this possibility, we analyzed DNA binding of different forms of recombinant Mre11 (WT, SA, SD) following incubation of *Xenopus* egg extracts with biotinylated linear DNA. As shown in Fig. 4A, substitution of S649/S688 with alanine resulted in a significant increase in Mre11 binding to DNA. In contrast, the DNA-binding ability of Mre11 was almost completely abolished upon introduction of aspartic acid mutations in S649 and S688 sites (Fig. 4A). Furthermore, pretreating recombinant WT GST-Mre11 with Plk1 and CK2 reduced the amounts of DNA-bound Mre11, but this effect was not observed when the S649A/S688A mutant was used (Fig. 4B). To further confirm that Mre11-S649/S688 phosphorylation regulates the Mre11/DNA binding, we performed electrophoretic mobility shift assay (EMSA) in a cell-free system. As shown in Fig. 4C and S4B, the binding of Mre11 to the 3′ overhang dsDNA was inhibited in Mre11-S649D, Mre11-S688D, and Mre11-S649D/S688D mutants, suggesting that the phosphorylation of Mre11 at S649 and S688 directly disrupts the Mre11/DNA complex. To validate these findings in intact cells, we examined the effect of Mre11 phosphorylation on the MRN complex recruitment to the DSBs. IF analysis showed that reconstitution of Mre11-depleted cells with Mre11-WT, but not the -S649D/S688D mutant, restores MRN complex recruitment to DSBs (Fig. 4D–F). Therefore, Mre11 phosphorylation at S649/S688 prevents the recruitment of the MRN complex to DSBs, likely due to reduced DNA binding ability of phosphorylated Mre11 (Fig. 4A–C).

Next, we asked whether the phosphorylation events affect the ATM signaling in response to DNA damage. As expected, DNA damage-induced activation of the ATM-Chk2 pathway was completely abolished upon Mre11 depletion (Fig. 4G, lanes 4–6). Reconstitution of Mre11-depleted cells with RNAi-resistant Mre11-WT completely rescued the phenotype (Fig. 4G, lanes 7–9). Of significance, cells expressing Mre11-S649D, Mre11-S688D, or Mre11-S649D/S688D mutants in the absence of endogenous Mre11 failed to activate the ATM/Chk2 pathway after DNA damage (Fig. 4G, lanes 10–12; Fig. 4H, lanes 2–4). To ensure that the finding is not IR specific, we repeated the experiment with doxorubicin. Again, cells expressing Mre11-WT and various S649/S688 to alanine mutants, but not S649/S688 to aspartic acid mutants, responded to doxorubicin to activate ATM and its targets Chk2 and H2AX (Fig. 4H).

To rule out the possibility that the reduced DNA binding of Mre11-SD mutants could result from an unstable MRN complex, we examined integrity of the MRN complex in cells expressing different forms of Mre11 (WT, SA, SD). 293T cells were transiently transfected with siRNA to deplete Mre11. Notably, silencing Mre11 also resulted in a significant reduction in protein levels of Rad50 and Nbs1 (Fig. S4C, compare lanes 1 and 2), which is consistent with a reduced expression of Nbs1 and Rad50 in the Mre11-deficient ATLD cells (29). This is because of a critical role of Mre11 to stabilize the MRN complex (30). In addition to the reduction of protein levels of Rad50 and Nbs1, there was also a reduction in Chk2 phosphorylation following IR when Mre11 was silenced (Fig. S4C, compare lanes 3

and 4). Then, we reintroduced RNAi-resistant GFP-Mre11 constructs (WT, −2A, −2D) and monitored MRN complex stability. As indicated in Figure S4D, expression of all three forms of GFP-Mre11 (WT, −2A, −2D) rescued the normal levels of Rad50 and Nbs1, ruling out the possibility that the MRN complex might be unstable in cells expressing Mre11-SD mutants. Further, we examined the interactions between different Mre11 variants and Rad50/Nbs1 and found that Mre11 mutants (2A, 2D) still co-immunoprecipitate with Rad50 and Nbs1 (Fig. S4E and F). To further investigate the potential role of Mre11-SD mutations in the MRN complex formation, we carried out IF studies. The HCT116 cells, which were Mre11 deficient, were transiently transfected with different forms of GFP-Mre11 mutants. IF analysis indicated that different Mre11 mutants can restore Nbs1 protein level (Fig. S4G). Collectively, we concluded that phosphorylation of Mre11 by Plk1 and CK2 does not affect the formation of the MRN complex.

Mre11-S649/S688 phosphorylation inhibits DNA repair

DSBs in eukaryotes are repaired by either homologous recombination (HR) or nonhomologous end joining (NHEJ), in which Mre11 is involved both. We examined the impact of Mre11-S649/S688 phosphorylation on the HR and NHEJ by utilizing two well-characterized GFP-based reporter systems: DR-GFP and EJ5-GFP. In brief, DR-GFP-HeLa or EJ5-GFP-HeLa cells were co-transfected with I-Scel-expressing vector and different Mre11 constructs (WT or S649D/S688D), and harvested for quantification of the GFP-positive population. Consistent with the previously reports, we found that Mre11 knockdown significantly decreased the fraction of GFP-positive cells (Fig. S4H). Interestingly, much higher DNA repair events were detected in cells expressing Mre11-WT compared to cells expressing Mre11-S649D/S688D (Fig. 5A and S4H), suggesting that phosphorylation of Mre11-S649/S688 inhibits DNA repair. Consistent with this observation, cells expressing Mre11-2D showed a markedly increased level of DNA damage than cells expressing Mre11-WT after 20 hr of repair incubation (Fig. 5B). Furthermore, cells expressing Mre11-2D also showed enhanced sensitivity to IR, indicated by both reduced cell survival (Fig. 5C) and colonial formation ability (Fig. 5D).

Considering that Mre11-defective cells had profound sensitivity to inhibitors of poly(ADP-ribose) polymerase (PARP) (31), we also investigated whether Mre11-S649/S688 phosphorylation affects the cellular response to Olaparib, a PARP inhibitor. Remarkably, cells expressing Mre11-WT and Mre11-2A variant exhibited significantly higher resistance to Olaparib compared to cells expressing Mre11-2D (Fig. 5E). Next, we compared the efficacy of Olaparib on xenograft tumors derived from U2OS cells expressing different forms of Mre11 (WT, 2A, 2D). Consistent with the in vitro data (Fig. 5E), tumors derived from Mre11-2D-expressing cells were much more sensitive to Olaparib than tumors derived from cells expressing Mre11-WT or −2A mutant (Fig. 5F–H).

Discussion

In this study, we show that 1) Plk1 phosphorylates Mre11 at S649 during G2 DNA damage recovery; 2) Plk1-mediated phosphorylation stimulates subsequent phosphorylation of Mre11 at S689 by CK2; and 3) Mre11 phosphorylation at S649/S689 drives premature

checkpoint termination and reduced DNA repair, thus likely contributing to IR-associated carcinogenesis.

It has been established that Plk1 is a key player of checkpoint recovery by phosphorylating several checkpoint factors, leading to their inactivation (14). The activity of Plk1 is required for inactivation of both ATM/Chk2 and ATR/Chk1 pathways. While Plk1 phosphorylation of Claspin leads to its degradation via $SCF^{\beta TRCP}$, thus inactivating the ATR/Chk1 pathway (13), the ATM-Chk2 pathway is also inactivated by Plk1 due to its phosphorylation of 53BP1 and Chk2 (14). More importantly, Plk1 is a predictive marker and therapeutic target for radiotherapy in rectal cancer (32). Despite these progress, whether Plk1 affects molecules upstream of ATM/ATR remains unknown. Herein, we show that Mre11 is a direct target of Plk1 and CK2 during the checkpoint recovery process. Based on our data, we propose the following working model. Upon DSB induction, the MRN complex is efficiently recruited to the site of damage and initiates damage response. Processed DNA lesions lead to the recruitment and activation of ATM, which in turn phosphorylates its substrates, among them Bora. Phosphorylated Bora is degraded in a $SCF^{\beta TrCP}$-dependent manner, resulting in Plk1 inactivation and cell cycle arrest at G2. During the subsequent recovery process, Plk1 phosphorylation of Mre11-S649 facilitates subsequent phosphorylation of Mre11-S688 by CK2, leading to MRN complex release from DNA and inactivation of both ATM-Chk2 and ATR-Chk1 pathways. In Plk1-overexpressing cells, Plk1 signaling impairs DDR by inhibiting the ATM pathway, likely due to reduced recruitment of the MRN complex to DNA damage. Considering that radiation is one major carcinogenetic factor, our data clearly demonstrate that the level/activity of Plk1 plays a critical role in IR-induced carcinogenesis for two reasons. First, elevation/activation of Plk1 causes premature termination of DNA damage checkpoint as we showed that Plk1 phosphorylation of Mre11 abolishes its binding ability to chromatin in response to DNA damage. Second, elevation/activation of Plk1 contributes to reduced DNA repair due to its phosphorylation toward Mre11. Altogether, a combination of premature termination of DNA damage checkpoint and reduced DNA repair will accelerate IR-associated carcinogenesis, suggesting that inhibition of Plk1 might be useful in prevention of IR-induced carcinogenesis.

It was previously described that Mre11 was phosphorylated at S649 both in vitro and in vivo, and in vitro kinase assay showed that Mre11-S649 was phosphorylated by CK2 (33). The unanswered questions were whether Mre11 S649 can be phosphorylated by CK2 in vivo and whether Mre11-S649 phosphorylation affects its function. It was established that both Plk1 and CK2 share the same sites in some substrates in vitro (26,27). Here we demonstrated that Mre11 was phosphorylated at S649 by Plk1 both in vitro and in vivo, and that depletion of Plk1, but not CK2, impaired S649 phosphorylation, supporting the notion that Plk1 is the major kinase that phosphorylates Mre11 at S649 in vivo. Finally, it was shown that phosphorylation of the C terminus of Mre11 was generally inhibitory to its functions (34). Consistent with this notion, we demonstrated that phosphorylation of Mre11-S649 impaires its binding to damaged DNA and suppresses DNA damage response pathway. Therefore, we identified a novel molecular mechanism that links Plk1, the MRN complex, and DDR.

Supplementary Material

Refer to Web version on PubMed Central for supplementary material.

Acknowledgments

This work was supported by NIH grants R01 CA157429 (X. Liu), R01 CA192894 (X. Liu), R01 CA196835 (X. Liu), R01 CA196634 (X. Liu), R01 AR059130 (N. Ahmad), R01 CA176748 (N. Ahmad), and R15 GM114713 (S. Yan). The work was also partially supported by Purdue University Center for Cancer Research (P30 CA023168).

Abbreviations

Plk1	Polo-like kinase 1
DDR	DNA damage response
MRN	Mre11/Rad50/Nbs1
DSBs	DNA double-strand breaks
HR	homologous recombination
NHEJ	non-homologous end-joining
GST	glutathione S-transferase
PBD	polo-box domain
PARP	poly(ADP-ribose) polymerase
ssDNA	single-stranded DNA
dsDNA	double-stranded DNA
DTB	double thymidine block
EMSA	electrophoretic mobility shift assay

References

1. Strebhardt K. Multifaceted polo-like kinases: drug targets and antitargets for cancer therapy. Nature reviews Drug discovery. 2010; 9(8):643–60. [PubMed: 20671765]
2. Liu X. Targeting Polo-Like Kinases: A Promising Therapeutic Approach for Cancer Treatment. Transl Oncol. 2015; 8(3):185–95. [PubMed: 26055176]
3. Smits VA, Klompmaker R, Arnaud L, Rijksen G, Nigg EA, Medema RH. Polo-like kinase-1 is a target of the DNA damage checkpoint. Nat Cell Biol. 2000; 2(9):672–6. [PubMed: 10980711]
4. van Vugt MA, Bras A, Medema RH. Polo-like kinase-1 controls recovery from a G2 DNA damage-induced arrest in mammalian cells. Mol Cell. 2004; 15(5):799–811. [PubMed: 15350223]
5. Huen MS, Chen J. Assembly of checkpoint and repair machineries at DNA damage sites. Trends Biochem Sci. 2010; 35(2):101–8. [PubMed: 19875294]
6. Paull TT, Gellert M. Nbs1 potentiates ATP-driven DNA unwinding and endonuclease cleavage by the Mre11/Rad50 complex. Genes & development. 1999; 13(10):1276–88. [PubMed: 10346816]
7. Paull TT, Gellert M. The 3′ to 5′ exonuclease activity of Mre 11 facilitates repair of DNA double-strand breaks. Molecular cell. 1998; 1(7):969–79. [PubMed: 9651580]

8. Zhuang J, Jiang G, Willers H, Xia F. Exonuclease function of human Mre11 promotes deletional nonhomologous end joining. The Journal of biological chemistry. 2009; 284(44):30565–73. [PubMed: 19744924]
9. Milman N, Higuchi E, Smith GR. Meiotic DNA double-strand break repair requires two nucleases, MRN and Ctp1, to produce a single size class of Rec12 (Spo11)-oligonucleotide complexes. Molecular and cellular biology. 2009; 29(22):5998–6005. [PubMed: 19752195]
10. Yata K, Lloyd J, Maslen S, Bleuyard JY, Skehel M, Smerdon SJ, et al. Plk1 and CK2 act in concert to regulate Rad51 during DNA double strand break repair. Mol Cell. 2012; 45(3):371–83. [PubMed: 22325354]
11. Qin B, Gao B, Yu J, Yuan J, Lou Z. Ataxia telangiectasia-mutated- and Rad3-related protein regulates the DNA damage-induced G2/M checkpoint through the Aurora A cofactor Bora protein. J Biol Chem. 2013; 288(22):16139–44. [PubMed: 23592782]
12. Macurek L, Lindqvist A, Lim D, Lampson MA, Klompmaker R, Freire R, et al. Polo-like kinase-1 is activated by aurora A to promote checkpoint recovery. Nature. 2008; 455(7209):119–23. [PubMed: 18615013]
13. Mamely I, van Vugt MA, Smits VA, Semple JI, Lemmens B, Perrakis A, et al. Polo-like kinase-1 controls proteasome-dependent degradation of Claspin during checkpoint recovery. Curr Biol. 2006; 16(19):1950–5. [PubMed: 16934469]
14. van Vugt MA, Gardino AK, Linding R, Ostheimer GJ, Reinhardt HC, Ong SE, et al. A mitotic phosphorylation feedback network connects Cdk1, Plk1, 53BP1, and Chk2 to inactivate the G(2)/M DNA damage checkpoint. PLoS Biol. 2010; 8(1):e1000287. [PubMed: 20126263]
15. Liu XS, Li H, Song B, Liu X. Polo-like kinase 1 phosphorylation of G2 and S-phase-expressed 1 protein is essential for p53 inactivation during G2 checkpoint recovery. EMBO reports. 2010; 11(8):626–32. [PubMed: 20577264]
16. Strebhardt K, Becker S, Matthess Y. Thoughts on the current assessment of Polo-like kinase inhibitor drug discovery. Expert Opin Drug Discov. 2015; 10(1):1–8. [PubMed: 25263688]
17. Lee KS, Burke TR Jr, Park JE, Bang JK, Lee E. Recent Advances and New Strategies in Targeting Plk1 for Anticancer Therapy. Trends Pharmacol Sci. 2015; 36(12):858–77. [PubMed: 26478211]
18. Willis J, DeStephanis D, Patel Y, Gowda V, Yan S. Study of the DNA damage checkpoint using Xenopus egg extracts. J Vis Exp. 2012; (69):e4449. [PubMed: 23149695]
19. Lee JH, Ghirlando R, Bhaskara V, Hoffmeyer MR, Gu J, Paull TT. Regulation of Mre11/Rad50 by Nbs1: effects on nucleotide-dependent DNA binding and association with ataxia-telangiectasia-like disorder mutant complexes. The Journal of biological chemistry. 2003; 278(46):45171–81. [PubMed: 12966088]
20. Olive PL, Banath JP. The comet assay: a method to measure DNA damage in individual cells. Nat Protoc. 2006; 1(1):23–9. [PubMed: 17406208]
21. Steegmaier M, Hoffmann M, Baum A, Lenart P, Petronczki M, Krssak M, et al. BI 2536, a potent and selective inhibitor of polo-like kinase 1, inhibits tumor growth in vivo. Curr Biol. 2007; 17(4): 316–22. [PubMed: 17291758]
22. Liu XS, Song B, Tang J, Liu W, Kuang S, Liu X. Plk1 phosphorylates Sgt1 at the kinetochores to promote timely kinetochore-microtubule attachment. Mol Cell Biol. 2012; 32(19):4053–67. [PubMed: 22869522]
23. van Attikum H, Gasser SM. Crosstalk between histone modifications during the DNA damage response. Trends in cell biology. 2009; 19(5):207–17. [PubMed: 19342239]
24. Chen C, Zhang L, Huang NJ, Huang B, Kornbluth S. Suppression of DNA-damage checkpoint signaling by Rsk-mediated phosphorylation of Mre11. Proceedings of the National Academy of Sciences of the United States of America. 2013; 110(51):20605–10. [PubMed: 24297933]
25. Iliuk A, Liu XS, Xue L, Liu X, Tao WA. Chemical visualization of phosphoproteomes on membrane. Mol Cell Proteomics. 2012; 11(9):629–39. [PubMed: 22593177]
26. Li H, Liu XS, Yang X, Wang Y, Turner JR, Liu X. Phosphorylation of CLIP-170 by Plk1 and CK2 promotes timely formation of kinetochore-microtubule attachments. Embo J. 2010; 29(17):2953–65. [PubMed: 20664522]
27. Wu ZQ, Liu X. Role for Plk1 phosphorylation of Hbo1 in regulation of replication licensing. Proc Natl Acad Sci U S A. 2008; 105(6):1919–24. [PubMed: 18250300]

28. Paull TT, Gellert M. A mechanistic basis for Mre11-directed DNA joining at microhomologies. Proc Natl Acad Sci U S A. 2000; 97(12):6409–14. [PubMed: 10823903]

29. Stewart GS, Maser RS, Stankovic T, Bressan DA, Kaplan MI, Jaspers NG, et al. The DNA double-strand break repair gene hMRE11 is mutated in individuals with an ataxia-telangiectasia-like disorder. Cell. 1999; 99(6):577–87. [PubMed: 10612394]

30. Olson E, Nievera CJ, Lee AY, Chen L, Wu X. The Mre11-Rad50-Nbs1 complex acts both upstream and downstream of ataxia telangiectasia mutated and Rad3-related protein (ATR) to regulate the S-phase checkpoint following UV treatment. The Journal of biological chemistry. 2007; 282(31): 22939–52. [PubMed: 17526493]

31. Koppensteiner R, Samartzis EP, Noske A, von Teichman A, Dedes I, Gwerder M, et al. Effect of MRE11 loss on PARP-inhibitor sensitivity in endometrial cancer in vitro. PloS one. 2014; 9(6):e100041. [PubMed: 24927325]

32. Rodel F, Keppner S, Capalbo G, Bashary R, Kaufmann M, Rodel C, et al. Polo-like kinase 1 as predictive marker and therapeutic target for radiotherapy in rectal cancer. Am J Pathol. 2010; 177(2):918–29. [PubMed: 20581060]

33. Kim ST. Protein kinase CK2 interacts with Chk2 and phosphorylates Mre11 on serine 649. Biochem Biophys Res Commun. 2005; 331(1):247–52. [PubMed: 15845385]

34. Di Virgilio M, Ying CY, Gautier J. PIKK-dependent phosphorylation of Mre11 induces MRN complex inactivation by disassembly from chromatin. DNA Repair (Amst). 2009; 8(11):1311–20. [PubMed: 19709933]

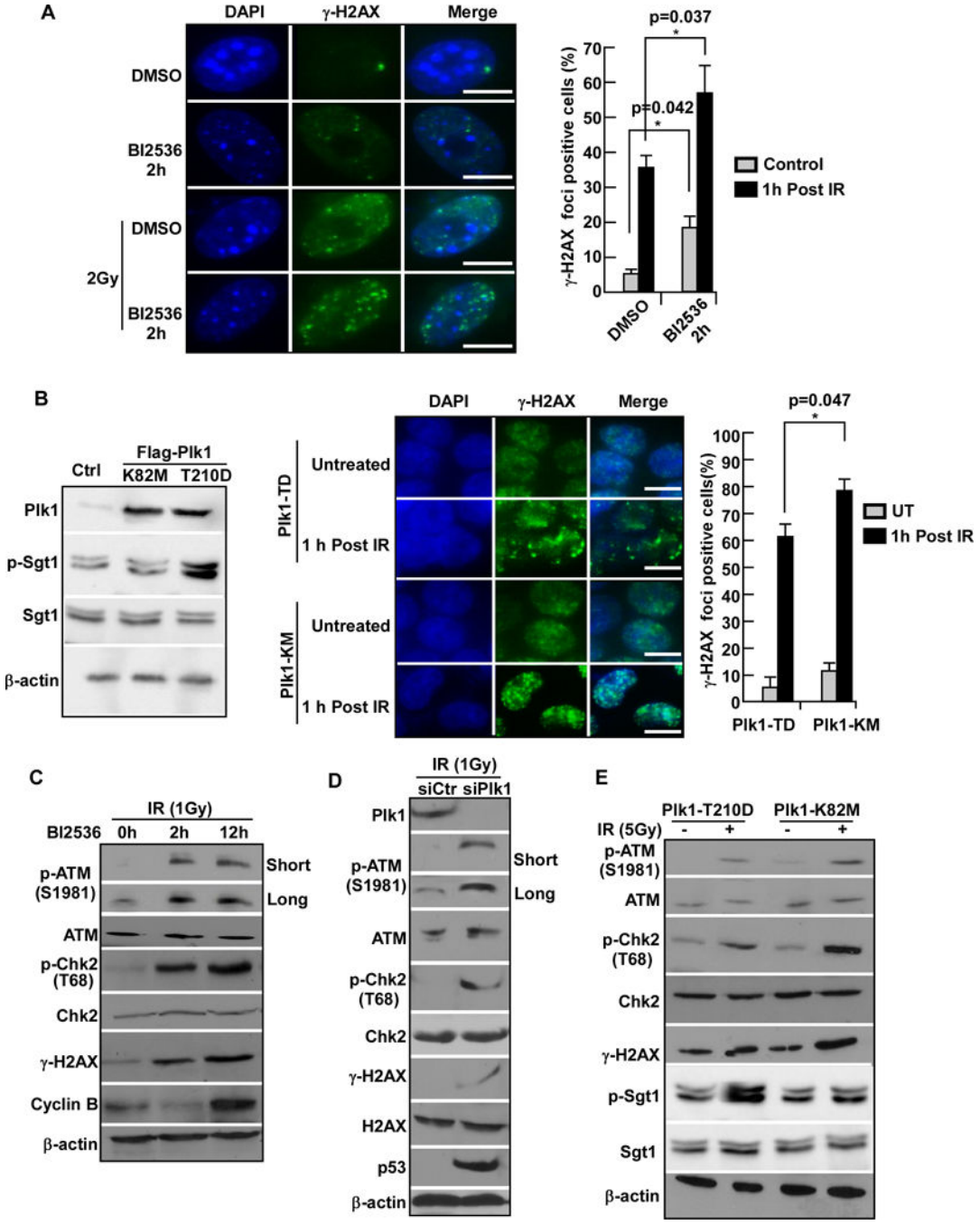

Figure 1.

Plk1 suppresses DDR by inactivation of the ATM-Chk2 pathway. A, U2OS cells were treated with 50 nmol/L of BI2536 for 2 hours, irradiated with 2 Gy γ-ray, and harvested at 1 hour post-radiation for γ-H2AX immunofluorescence (IF) staining. For quantification, at least 300 cells were scored for γ- H2AX foci and percentages of cells with 5 or more foci are shown. Values are mean ± s.d. of three independent experiments. *: $P < 0.05$ (two-tailed unpaired t-test). Scale bars: 5 μm. B, U2OS cells were transfected with different Flag-Plk1 constructs (K82M, kinase dead form; T210D, constitutively active form), treated with 2 Gy

IR, incubated for 1 hour, and harvested for immunoblotting (IB, left) or γ-H2AX staining (middle). At least 300 cells were counted for γ-H2AX foci and percentages of cells with 5 or more foci are shown (right). Values are mean ± s.d. of three independent experiments. *: $P < 0.05$. Scale bars: 10 μm. C-E, Plk1 is involved in inactivation of the ATM-Chk2 signaling. C, U2OS cells were treated with 50 nmol/L BI2536 for the indicated times, exposed to 1 Gy of IR, and harvested. D, U2OS cells were transfected with the indicated siRNA for 2 days and exposed to 1 Gy of IR. E, U2OS cells were transfected with Plk1 constructs and irradiated with 5 Gy γ-ray.

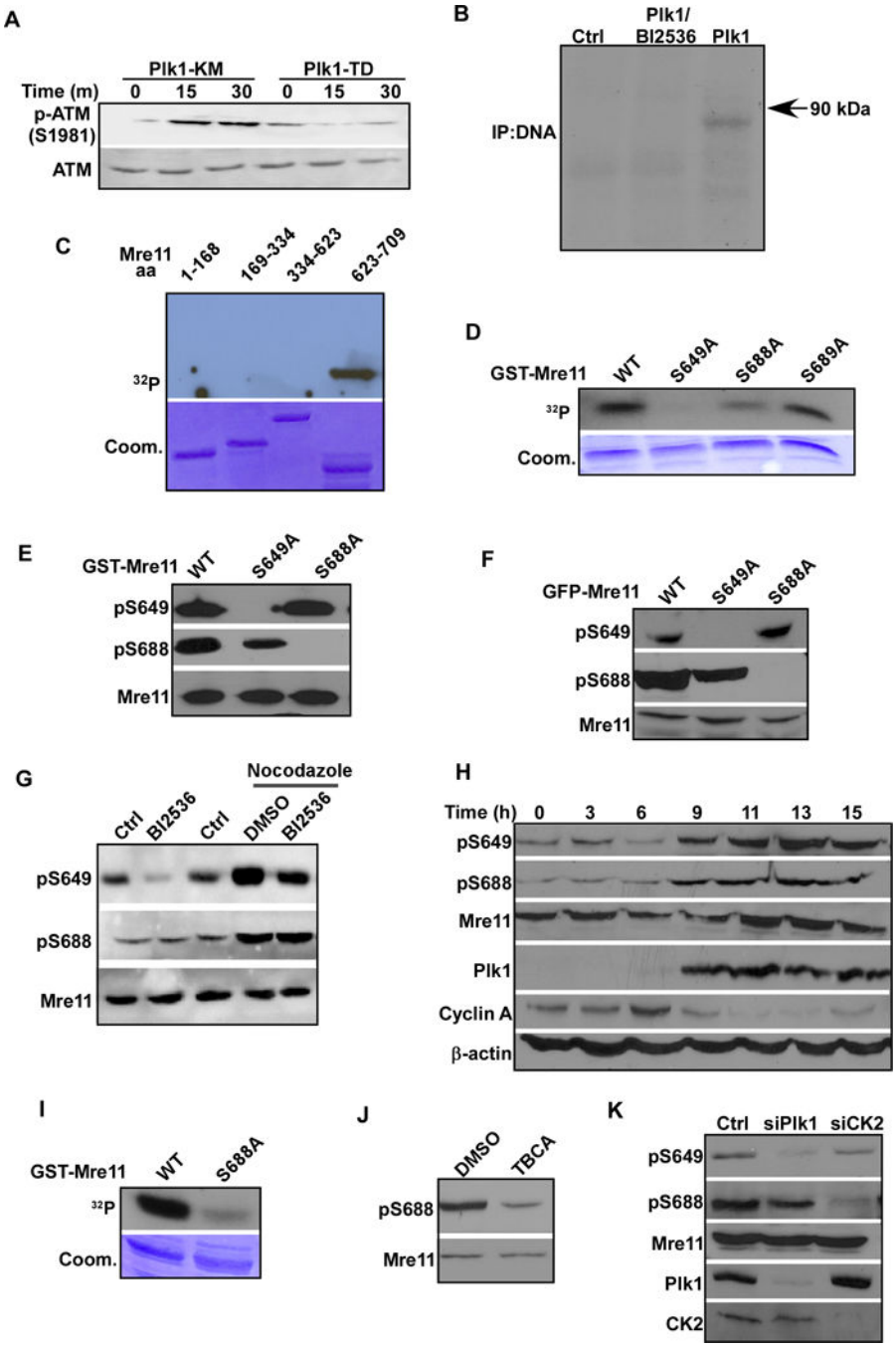

Figure 2.

Plk1 phosphorylates Mre11 at S649. A, Plk1 inhibits ATM autophosphorylation. *Xenopus* oocyte extracts were incubated with constitutively active or kinase-dead Plk1 for 30 minutes before the addition of dsDNA and ATM protein that was immunoprecipitated from HeLa cells. Reactions were terminated at indicated times. B, biotin tagged-dsDNA was bound to avidin beads, then incubated with *Xenopus* oocyte extracts for 30 minutes. After washing with egg lysis buffer, beads were incubated with purified Plk1 in the presence of [γ-^{32}P]ATP, followed by autoradiography. C, Plk1 phosphorylates Mre11 in vitro. After

purified Plk1 was incubated with purified GST-Mre11 regions in the presence of [γ-^{32}P]ATP, the reaction mixtures were resolved by SDS-PAGE, stained with Coomassie brilliant blue (Coom.), and detected by autoradiography. D, Plk1 phosphorylates Mre11 S649 and S688 in vitro. Plk1 was incubated with GST-Mre11 (WT, S649A or S688A) as in C. E, the pS649-Mre11 and pS688-Mre11 antibodies are specific. Plk1 was incubated with GST-Mre11 (WT, S649A or S688A) in the presence of unlabeled ATP, followed by anti-pS649-Mre11 or anti-pS688-Mre11 IB. F, S649 and S688 of Mre11 are phosphorylated in vivo. 293T cells were transfected with GFP-Mre11 constructs (WT, S649A or S688A). G, endogenous Plk1 phosphorylates endogenous Mre11 at S649. 293T cells were treated with nocodazole for 12 hours, followed by incubation with BI2536 for additional 12 hours. H, temporal regulation of Mre11 phosphorylation. HeLa cells were synchronized by the DTB protocol to arrest at G1/S boundary and released for different times. I, CK2 phosphorylates Mre11 at S688 in vitro. Purified CK2 was incubated with GST-Mre11 (WT or S688A) as in C. J, endogenous CK2 phosphorylates endogenous Mre11 at S688. 293T cells were treated with TBCA for 12 hours. K, Plk1 and CK2 are responsible for S649 and S688 phosphorylation in vivo, respectively. 293T cells were transfected with pBS/U6-Plk1 to deplete Plk1 or pKD-CK2 to deplete CK2.

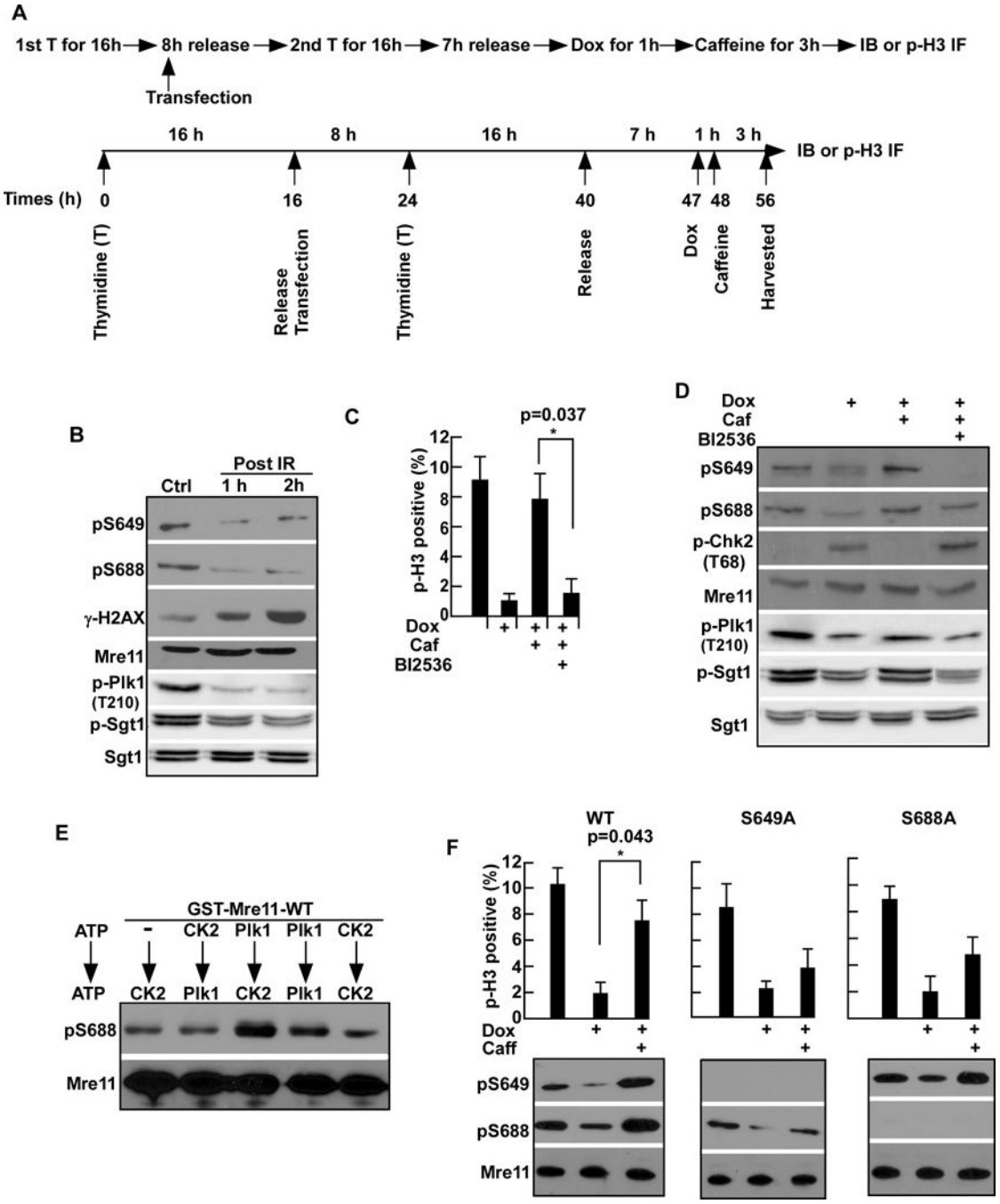

Figure 3.

Phosphorylation of Mre11 by Plk1 and CK2 is required for G2 DNA damage checkpoint recovery. A, schematic to study the role of Plk1/CK2-mediated phosphorylation of Mre11 during G2 DNA damage checkpoint recovery. U2OS cells were treated with thymidine for 16 hours to arrest at the G1/S boundary and released by washing away of thymidine. After 8 hours of release [if required, cells were transfected with indicated plasmids at the beginning of release (Fig. 3F)], cells were treated with second round of thymidine for 16 hours to arrest at the G1/S boundary, and then released into fresh medium for 7 hours to enrich at G2 phase,

followed by exposure with IR or treatment with doxorubicin for 1 hour. Upon doxorubicin removal, cells were released for additional 3 hours ± caffeine ± BI 2536 and harvested for IB or phospho-H3 (p-H3) staining. B, U2OS cells synchronized as in A were exposed to 5 Gy of IR and harvested at indicated times. C, U2OS cells processed as in A were analyzed for p-H3 staining. D, cells as described in A were analyzed for IB. E, purified GST-Mre11 was incubated with CK2 or Plk1 in the presence of unlabeled ATP, then incubated with CK2 or Plk1 again in the presence of unlabeled ATP. F, U2OS cells expressing RNAi-resistant Mre11 constructs (WT, S649A or S688A) were processed as in A with endogenous Mre11 was depleted during the 8 hours interval, and harvested to monitor mitotic entry (top) and Mre11 phosphorylation (bottom).

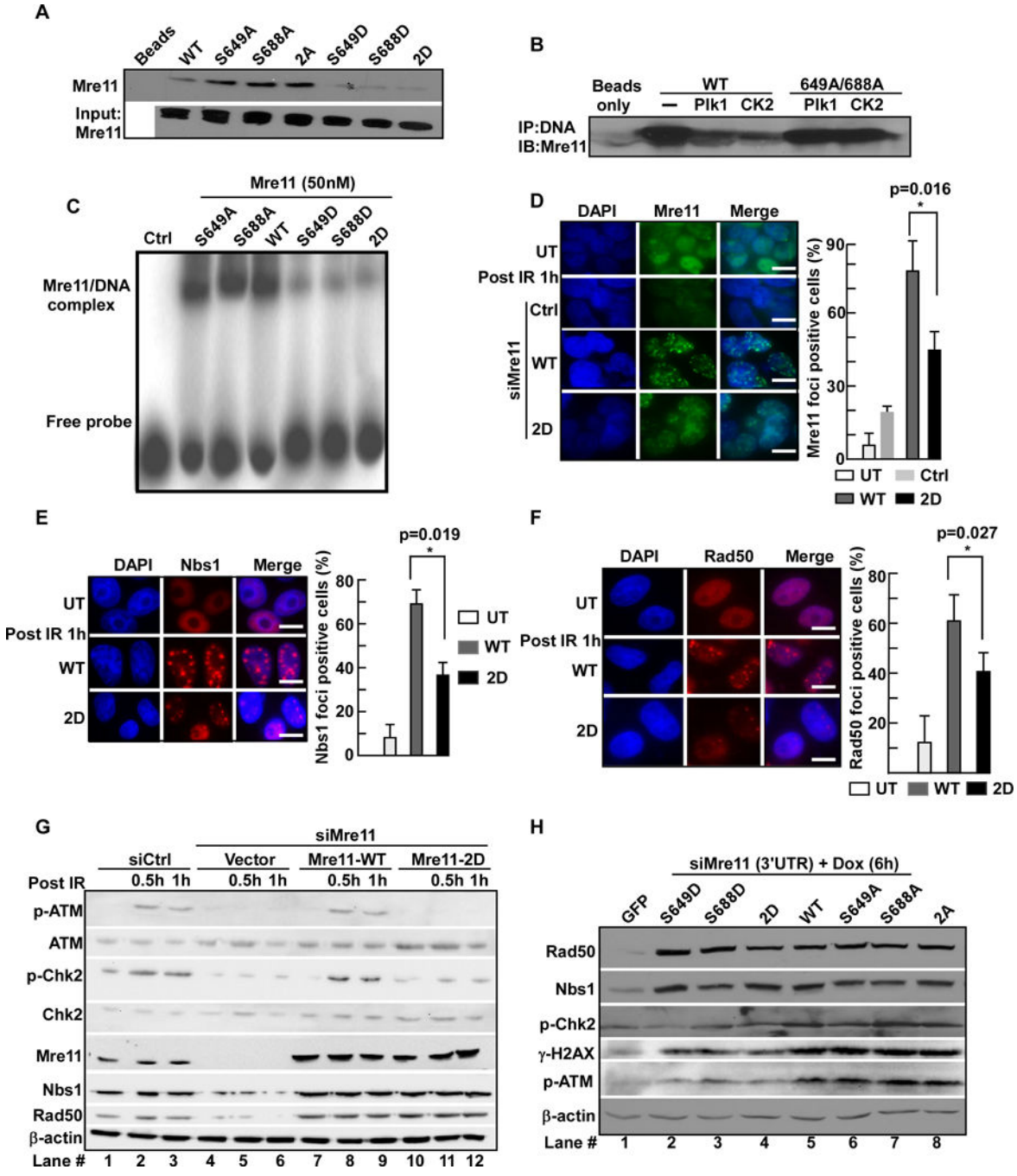

Figure 4.

Mre11-S649/S688 phosphorylation inhibits its binding to dsDNA and impairs ATM signaling. A-C, phosphorylation of Mre11 on S649 and S688 reduces its binding to DNA. A, after *Xenopus* egg extracts supplemented with purified WT or mutant Mre11 proteins were incubated with biotin-tagged dsDNA-bound avidin beads, pellets were analyzed for Mre11 IB. 2A: S649A/S688A; 2D: S649D/S688D. B, purified Mre11 (WT or S649A/S688A) proteins were treated with Plk1 or CK2 for 10 min, incubated with biotin-tagged dsDNA-bound avidin beads for 30 min, and processed as in A. C, EMSA assay of Mre11 variants on

dsDNA. ^{32}P-labelled 3′ overhanging DNA duplexes were incubated with Mre11 mutants and subjected to EMSA. D-F, U2OS cells reconstituted with RNAi-resistant Mre11 constructs (WT or S649D/S688D) were exposed to 3 Gy of IR, incubated for 1 hour, and subjected to IF with antibodies against Mre11 (D), Nbs1 (E), and Rad50 (F). Bars represent mean ± s.d. (n = 3). G and H, Mre11 S649 and S688 phosphorylation impairs ATM signaling. G, Mre11-depleted U2OS cells were reconstituted with RNAi-resistant Mre11 (WT or S649D/S688D) constructs, exposed to 3 Gy of IR, and harvested at indicated times. H, Mre11-depleted U2OS cells were reconstituted with RNAi-resistant WT or various Mre11 mutants and exposed to doxorubicin for 6 hours.

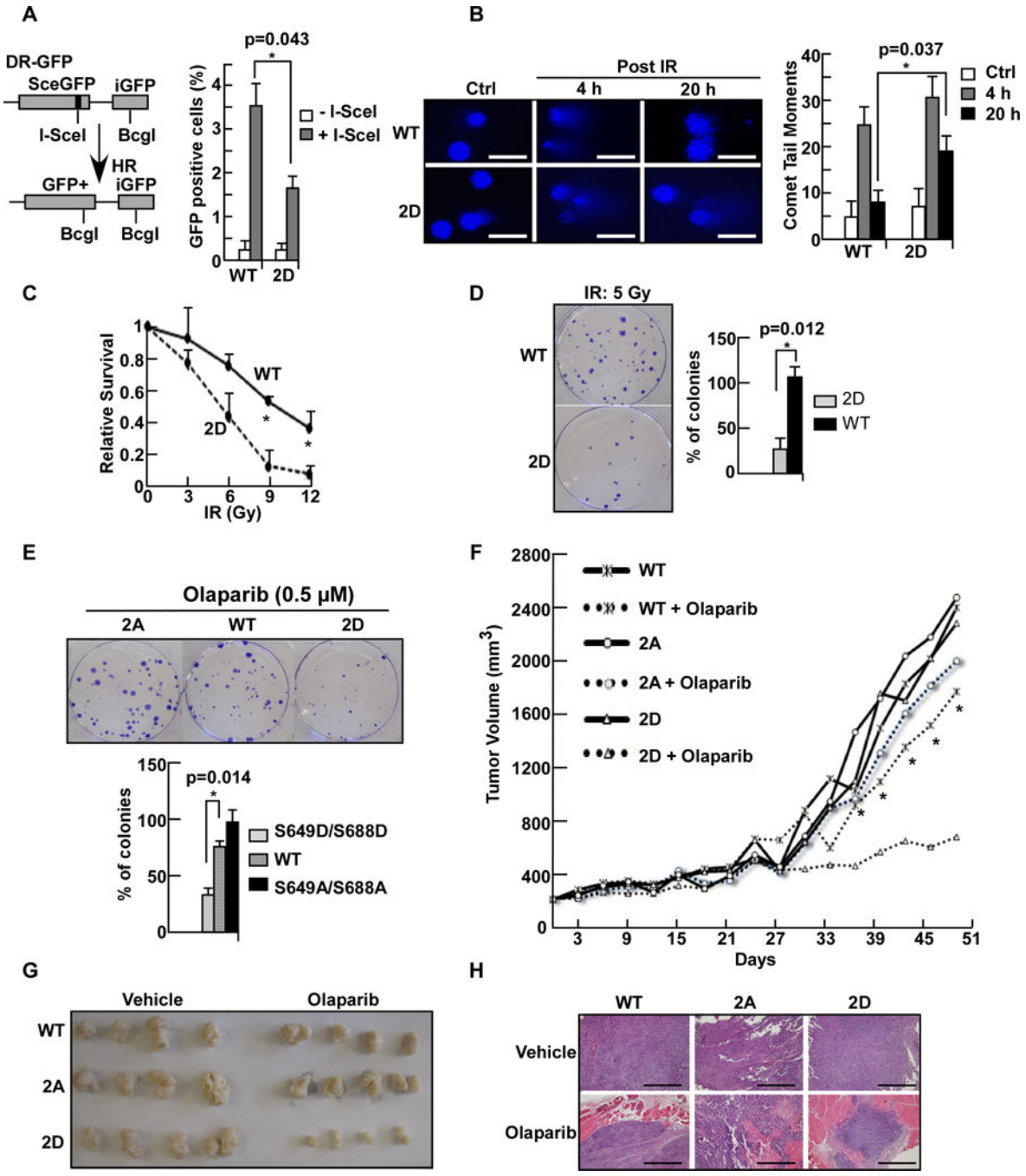

Figure 5.

Mre11-S649/S688 phosphorylation inhibits HR repair. A, Left, schematic representation depicting the inter-sister HR assay using tandem GFP substrates. The DR-GFP reporter contains an I-SceI endonuclease cleavage site within the coding region of a GFP gene (SceGFP). Downstream of SceGFP and in the same orientation is a 0.8 kb truncated GFP gene (iGFP), which can template the repair of the DSB in the SceGFP gene to restore functionality of the GFP gene. Right, relative intensities of GFP signal following I-SceI expression in cells expressing Mre11 constructs (WT or 2D) are shown. Error bars, SD (n =

3). B-D, Mre11-S649/S688 phosphorylation impairs HR repair and cell survival. B, U2OS cells were depleted of Mre11, transfected with RNAi-resistant Mre11 (WT or 2D), exposed to IR, and harvested at different times for alkaline comet assay to monitor DNA damage. Scale bars: 20μm. C, U2OS cells with endogenous Mre11 was replaced with RNAi-resistant Mre11 (WT or 2D) were exposed to the indicated doses of IR for 3 days, and subjected for MTT assay. D, fourteen days after cells as in C were treated with 5 Gy IR, colonies were fixed and stained with hematoxylin. Error bars represent the standard deviations of the means of 3 independent experiments. E, U2OS cells expressing various Mre11 (WT, 2A, 2D) constructs were exposed to 0.5 μmol/L Olaparib for 14 days and subjected to clonogenic survival assay. F, U2OS cells expressing different forms of Mre11 (WT, 2A, 2D) were used to grow tumors subcutaneously (4 mice per group). When the tumors reached the sizes of 200–220 mm^3, mice were treated with Olaparib for 51 days. G, final tumor sizes of F. H, H&E staining of tumors from F. Scale bars:20μm.